# In-phantom film measurements of two treatment planning systems for single-fraction spine SBRT

Michael Taylor[1], Jonas Fontenot, PhD[2]

(1) mtay153@lsu.edu, Louisiana State University; (2) jfontenot@marybird.com, Mary Bird Perkins Cancer Center

## Background

Radiation therapy is an effective palliative treatment method for cancers in the spinal region, but overdosing the spinal cord can cause severe side effects.[1] Stereotactic body radiation therapy (SBRT) can prevent these with its high conformity, dose gradient, and biological effective dose. Radiotherapy delivery accuracy is influenced by the dose calculation algorithm of the treatment planning system (TPS). Two such dose calculation algorithms in use are convolution superposition (CS) models and Monte Carlo (MC) based algorithms. Although both methods produce clinically acceptable plans,[2,3] previous studies have found that MC-based algorithms generally yield a more accurate calculation than CS-based at tissue-to-bone interfaces.[1,4] The goal of this study was to investigate and compare the end-to-end dosimetric accuracy of a CS-based TPS and MC-based TPS for spine SBRT treatments. The hypothesis was that, for single-fraction spine SBRT treatments, the MC-based TPS would calculate the critical dose gradient between the vertebral body and spinal cord more accurately than the CS-based TPS when compared to in-phantom film measurements.

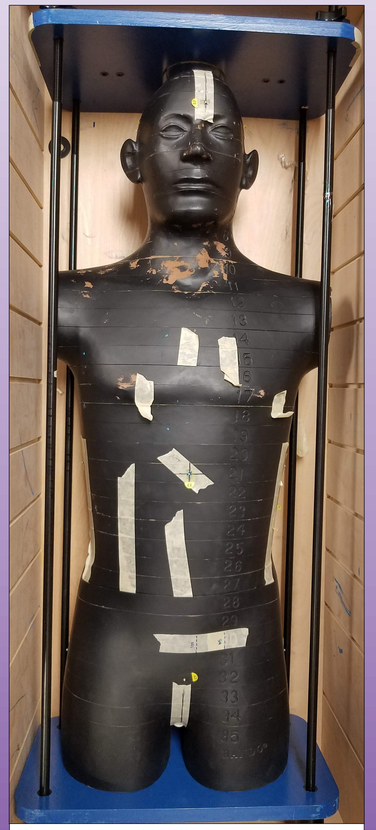

**Figure 1.** Alderson RANDO anthropomorphic phantom, consisting of bone, soft-tissue, and lung equivalent material.

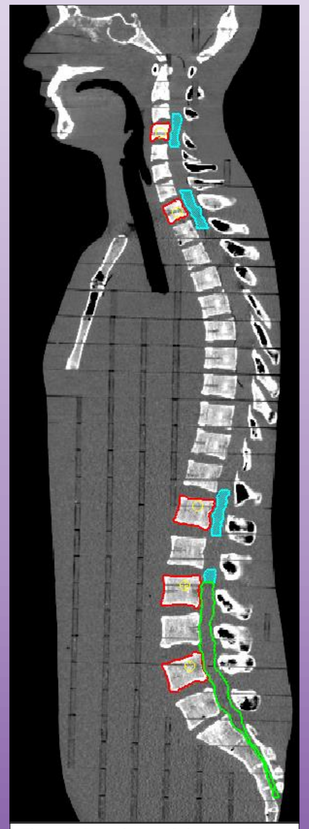

**Figure 2.** Sagittal view of phantom CT scan, with the treated vertebral sites, spinal cord, and cauda equina contoured in red, blue, and green, respectively.

## Methods & Materials

The Alderson RANDO anthropomorphic phantom[5] (**Figure 1**) was CT scanned and imported into two TPSs, Philips Pinnacle3 ($TPS_{CS}$) and Elekta Monaco ($TPS_{MC}$). Following ROTG-0631 guidelines,[6] single-fraction 6 MV flattening filter free dual-arc VMAT treatment plans were optimized and calculated (2 mm dose grid) at 5 vertebral sites in each TPS: C4, T1, T12, L2, and L4 (**Figure 2**). Each plan was then delivered over three trials with an Elekta Versa HD linear accelerator to Gafchromic EBT-XD film inserted in the phantom at each site. The films were scanned in an Epson Expression 10000XL flatbed scanner at least 48 hours post-irradiation, then anterior-posterior (AP) dose profiles on the TPS-calculated dose planes and the respective mean RGB film-measured dose planes were obtained (**Figure 3**). 2D gamma pass rate (GPR) at multiple dose difference / distance to agreement (ΔD/DTA) criteria was also performed on all film scans in a limited region of interest (ROI).[7] TG-119 IMRT plans were also calculated in each TPS and delivered to a MapCHECK2 diode array to obtain qualitative baseline GPRs.[8]

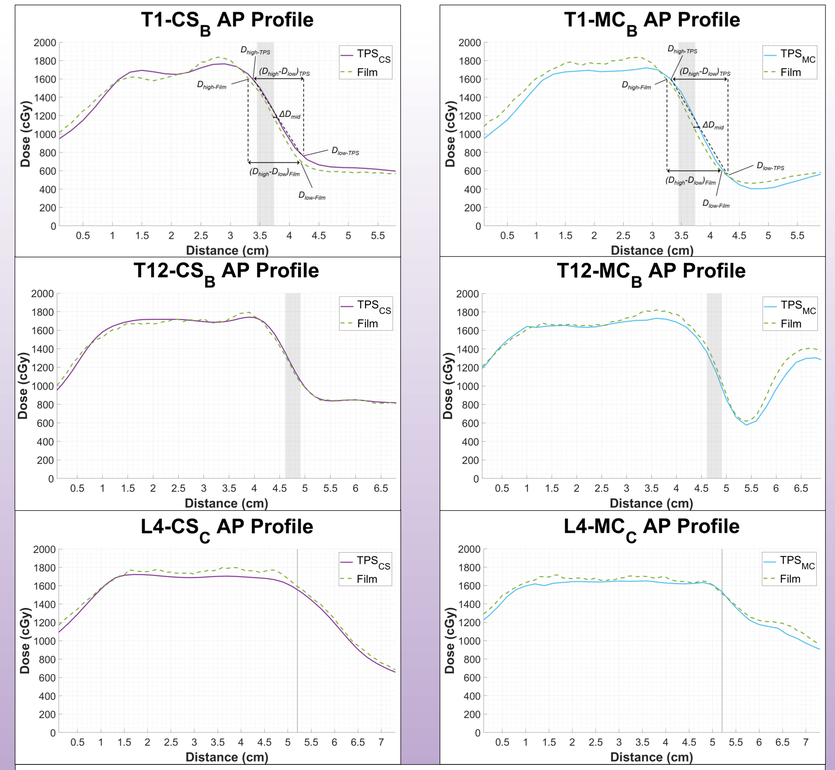


**Figure 3.** AP dose profiles for T1, T12, and L4 trials of $TPS_{CS}$ and $TPS_{MC}$ with their respective film profiles. Points of interest for the profile metrics are labeled on the T1 profiles. The shaded areas represent the region from the PTV edge to the cord/cauda edge.

## Results

On each TPS and film dose profile, two positions, $D_{high}$ and $D_{low}$, were first determined. $D_{high}$ was defined as the last position of the 1600 cGy dose value before the dose falloff began. $D_{low}$ was defined as the first position that reaches a threshold dose gradient of -500 cGy/cm after the negative slope began (for the L4 $TPS_{MC}$ plans, this threshold was -200 cGy/cm). The dose falloff difference (**Table 1**) was defined as the distance from $D_{high}$ to $D_{low}$ on the TPS profile subtracted from the same distance on the film profile. The isodose shift, $\Delta D_{mid}$, (**Table 2**) was defined as the midpoint of $D_{high}$ and $D_{low}$ on the TPS profile subtracted from the position that matches that dose value on the film profile. After confirming normality and equal variances between the TPS samples, a two-tailed, unpaired, equal variance t-test ($n = 5$, $\alpha = 0.05$) was conducted, showing no statistically significant difference between the TPSs for these profile metrics. $TPS_{CS}$ consistently obtained greater mean GPR than $TPS_{MC}$ across all sites (**Figure 4**). Normality was confirmed, equality of variance was determined, then each ΔD/DTA sample of GPR received the appropriate two-tailed, unpaired t-test (either equal or unequal variance). The differences in GPR between each TPS were statistically significant for all criteria all except 2%/1mm and 1%/1mm.

| Treatment Planning System | C4 | T1 | T12 | L2 | L4 | Site Mean Falloff Difference | Standard Deviation | p-value |
|---|---|---|---|---|---|---|---|---|
| $TPS_{CS}$ (mm) | -0.3 | +0.6 | -0.3 | +0.8 | -1.1 | **+0.0** | 0.8 | 0.167 |
| $TPS_{MC}$ (mm) | -0.4 | -0.1 | -0.5 | -0.8 | -1.5 | **-0.7** | 0.5 | |
| $TPS_{CS}$ (%) | -2.9 | +7.1 | -3.5 | +10.7 | -7.8 | **+0.7** | 7.8 | 0.088 |
| $TPS_{MC}$ (%) | -5.1 | -1.3 | -5.2 | -11.0 | -16.6 | **-7.8** | 6.0 | |

**Table 1.** AP dose falloff differences and percent differences between the TPS-calculated and film-measured profiles of $TPS_{CS}$ and likewise for $TPS_{MC}$. Each value under the treatments sites is the average of the three trials for that site. Differences of 0 mm or 0% are ideal. A positive difference indicates the film profile had a more gradual dose falloff relative to the TPS profile, and a negative difference indicates a sharper falloff. The p-value is the result of a two-tailed, unpaired, equal variance t-test.

| Treatment Planning System | C4 | T1 | T12 | L2 | L4 | Site Mean Shift | Standard Deviation | p-value |
|---|---|---|---|---|---|---|---|---|
| $TPS_{CS}$ (mm) | +0.2 | -0.6 | -0.3 | -0.2 | 0.3 | **-0.1** | 0.3 | 0.655 |
| $TPS_{MC}$ (mm) | -0.3 | -0.9 | +0.4 | 0.2 | +0.7 | **+0.0** | 0.6 | |

**Table 2.** AP isodose shifts ($\Delta D_{mid}$) between the TPS-calculated and film-measured profiles of $TPS_{CS}$ and likewise for $TPS_{MC}$. Each value under the treatments sites is the average of the three trials for that site. A shift of 0 mm is ideal. A positive value indicates the film profile is shifted posterior to the TPS profile, and a negative value is an anterior shift. The p-value is the result of a two-tailed, unpaired, equal variance t-test.

## Discussion

Across all sites, the most common area for pixels to fail gamma criteria 2%/2mm was inside the PTV, specifically in the posterior portion. $TPS_{MC}$ consistently had more failing pixels inside the PTV compared to $TPS_{CS}$. $TPS_{MC}$ also had failing pixels immediately posterior to the spinal cord and cauda equina for all sites except C4 (**Figures 5 and 6**). Such failures occurred minorly in $TPS_{CS}$ at the T1 site. The critical pixels between the posterior PTV edge and anterior cord/cauda edge generally failed once the at 1 mm DTA (with 5%/1mm being the exception). Pixels near the edge of their ROI tended to fail for both TPSs. The TG-119 IMRT plans made in each TPS and delivered to the diode array showed that the most common area of failure was also inside the targets (2%/2mm criteria). For most of the plans, $TPS_{MC}$ delivered around twice the number of MU and defined more VMAT control points compared to the plans to $TPS_{CS}$. The minimum segment width was also set, by default, smaller than $TPS_{CS}$. The resulting higher modulation possibly pushed the linear accelerator to its limits, yielding lower GPR for $TPS_{MC}$.[9]

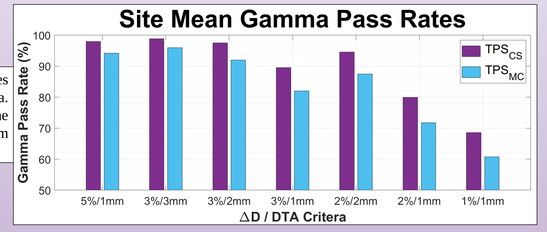


**Figure 4.** Mean GPR across all treatment sites for each TPS across multiple ΔD/DTA criteria. Each ΔD is based on a percentage of the maximum planned dose. A 10% maximum planned dose threshold was also applied.

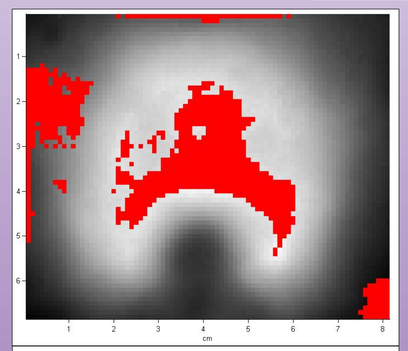

**Figure 5.** Scanned film dose plane of the **T12** $TPS_{CS}$ plan, Trial C, with red pixels failing 2%2mm criteria.

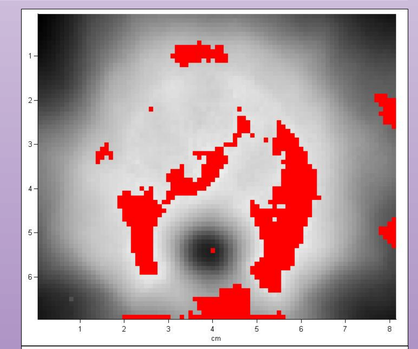

**Figure 6.** Scanned film dose plane of the **T12** $TPS_{MC}$ plan, Trial C, with red pixels failing 2%2mm criteria.

## Conclusion

In the critical region of the selected vertebral sites, there was no significant difference in dose falloff or isodose shift between each TPS-calculated dose distribution and their respective film-measured dose distributions. The lower GPR seen in $TPS_{MC}$ warrants further investigation. Suggestions include directly transferring the optimized VMAT segments from $TPS_{CS}$ to $TPS_{MC}$ and examining relationships between the IMRT optimization settings of $TPS_{MC}$ and its measurements.

## Conflict of Interest

This project was funded by Elekta Limited.

## References

[1] Rijken J, Crowe S, Trapp J, Kairn T. A review of stereotactic body radiotherapy for the spine. Phys. Eng. Sci. Med. 2020; 43(3): 799–824.
[2] Lee YK, Munawar I, Mashouf S, Sahgal A, Ruschin M. Dosimetric comparison of two treatment planning systems for spine SBRT. Med. Dosim. 2020; 45(1): 77–84.
[3] Saenz DL, Crownover R, Stathakis S, Papanikolaou N. A dosimetric analysis of a spine SBRT specific treatment planning system. J. Appl. Clin. Med. Phys. 2019; 20(1): 154–159.
[4] Paudel MR, Kim A, Sarfehnia A, et al. Experimental evaluation of a GPU-based monte carlo dose calculation algorithm in the Monaco treatment planning system. J. Appl. Clin. Med. Phys. 2016; 17(6): 230–241.
[5] Alderson SW, Lanzl LH, Rollins M, Spira J. An instrumented phantom system for analog computation of treatment plans. Am. J. Roentgenol. Radium Ther. Nucl. Med. 1962; 87: 185–195.
[6] Ryu S, Gerszten P, Yin F-F, et al. Radiation Therapy Oncology Group RTOG 0631 Phase II / III Study of Image-Guided Radiosurgery/SBRT for Localized Spine Metastasis. 2010;
[7] Ju T, Simpson T, Deasy JO, Low DA. Geometric interpretation of the γ dose distribution comparison technique: Interpolation-free calculation. Med. Phys. 2008; 35(3): 879–887.
[8] Ezzell GA, Burmeister JW, Dogan N, et al. IMRT commissioning: Multiple institution planning and dosimetry comparisons, a report from AAPM Task Group 119. Med. Phys. 2009; 36(11): 5359–5373.
[9] Miften M, Olch A, Mihailidis D, et al. Tolerance limits and methodologies for IMRT measurement-based verification QA: Recommendations of AAPM Task Group No. 218. Med. Phys. 2018; 45(4): e53–e83.